Proceedings of the 3rd
RSI International Conference on Robotics and Mechatronics
October 7-9, 2015, Tehran, Iran

Vision-Based Kinematic Calibration of Spherical Robots

Pedram Agand, Hamid D. Taghirad *Senior Member, IEEE and Amir Molaee*

Advanced Robotics and Automation System (ARAS), Industrial Control Center of Excellence (ICEE), Department of Systems and Control, Faculty of Electrical Engineering, K. N. Toosi University of Technology, Iran. (e-mail:Taghirad@kntu.ac.ir, aagand@email.kntu.ac.ir)

***Abstract*—In this article, a method to obtain spatial coordinate of spherical robot's moving platform using a single camera is proposed, and experimentally verified. The proposed method is an accurate, flexible and low-cost tool for the kinematic calibration of spherical-workspace mechanisms to achieve the desired accuracy in position. The sensitivity and efficiency of the provided method is thus evaluated. Furthermore, optimization of camera location is outlined subject to the prescribed cost functions. Finally, experimental analysis of the proposed calibration method on ARAS Eye surgery Robot (DIAMOND) is presented; In which the accuracy is obtained from three to six times better than the previous calibration.**

***Keywords*—Kinematic Calibration, Vision-Base Positioning, Eye Surgery Robot, Spherical Workspace.**

I. Introduction

In high-performance control system, that are of essential principle in delicate applications, a meticulous model of the system is required [1]. As one may not completely rely on the kinematic of robot, it is necessary to find the position of the robot end-effector independent of the robot structure. Compared to serial mechanisms, parallel structures may exhibit a much better repeatability, but their large number of links and passive joints often limits their performance in terms of accuracy [2], and therefore, a kinematic calibration is thus needed. The forward kinematic model of parallel structures can rarely be expressed analytically. The use of this model to achieve kinematic calibration may consequently lead to numerical instability [3]. On the other hand, the inverse kinematic model can usually be easily derived. Calibration can then be performed by comparing the measured joint variables and their corresponding values estimated from the measured end-effector pose and the inverse kinematic model. Each limb can furthermore, be calibrated independently. Up to now, the inverse kinematic model method seems to be the most efficient method performed [4]. Vision-based positioning is believed to be the most promising but challenging technology so far to determine the position and possibly the orientation of a vision system [5]. Vision based positioning or localization uses the same basic principles of landmark-based and map-based positioning but relies on optical sensors rather than ultrasound, dead-reckoning and inertial sensors. Real world applications envisaged in most current research projects however, demand more detailed sensor information to provide the robot with better environment-interaction capabilities [6]. For a successful accomplishment of off-line programming, the robots need to be not only repeatable but also accurate. Robot repeatability is unaffected by the method of programming since it is due to random errors (e.g. due to the finite resolution of joint encoders). In contrast, the systematic errors in absolute position are almost entirely due to off-line programming of the robot. Robot constant-pose errors are attributed to several sources, including errors in geometrical parameters (e.g. link lengths and joint offsets) and deviations which vary predictably with position (e.g. compliance or gear transmission errors) [7], [8]. The measurement step of the calibration process is necessary for the determination of the 'best fit' set of parameters to the actual robot. Vision-based measurement systems using a single camera for robot calibration seem to be one of the feasible methods in robot calibrations [2]. However, the knowledge produced in this area is still restricted to research groups.

In this paper a simple but efficient method to allocate a point in spherical coordinate (γ, ϕ) is proposed by assuming that the point is constrained to move on the surface of a sphere with a specific radius. Further precision and sensitivity of measurement based on camera parameter and scene configuration is calculated. As a case study we consider a spherical parallelogram robot in eye surgeries suggested by ARAS. In many surgeries it is necessary to rotate tools about a fixed pivot point such as Minimally Invasive Surgeries (MIS) [9]. Therefore, remote center of motion (RCM) mechanism, provided by almost all spherical manipulator, are recommended for most of medical robots [10], [11]. We reinforce this inherent property of the robot using prescribe method of calibration.

II. Kinematic Calibration

In this section, the preliminaries for calibration of a mechanism using vision-based metrology is given. It is shown that one must introduce additional parameters owing to the use of an exteroceptive measurement of the end-effector pose [12]. The requirements of a singularity-free parameter identification model prevents the use of a single modeling convention that can be applied uniformly to all possible robot geometries [13].

Contrary to serial mechanisms, the inverse kinematic model of parallel mechanisms can often be expressed analytically [3]. It computes the joint variables q_c as a function of the moving platform pose in screw coordinates; based on Chasles' theorem one may write:

$$^{A}P_e = \$ = \begin{bmatrix} \hat{s} \\ s_0 \times \hat{s} + \lambda \hat{s} \end{bmatrix} \tag{1}$$

Where $\lambda = \dot{d}/\dot{\theta}$ denotes the pitch of motion. With his general motion definition with kinematic parameters ζ_k the following

978-1-4673-7234-3/15/$31.00 ©2015 IEEE

error can be formed:

$$\epsilon_i = \tilde{q}_i - q_c(\$, \zeta_k) \tag{2}$$

The error is formed between the corresponding measured joint values $\tilde{q}_i$ and the computed ones $q_c(\$, \zeta_k)$. We propose to estimate ζ_k by a nonlinear optimization problem that minimizes the variance of the error in presence of measurement Gaussian noise:

$$J(\zeta_k) = \epsilon^T \epsilon, \quad \epsilon = (\epsilon_1^T, ..., \epsilon_m^T)^T \tag{3}$$

However, this suggests that the end-effector pose can be measured in the base frame. Due to the use of an exteroceptive measuring device, in fact, the measurement is relative with respect to the pose of the measuring device with respect to the base frame ${}^A P_c$. Formally this implies that one measures poses of the target with respect to the measuring device ${}^c P_t$ which are related to the end-effector poses with respect to the base by the unknown constant transformations ${}^A T_c$ so [14]:

$${}^A P_e = {}^A T_c \ {}^c P_t \ {}^t T_e \tag{4}$$

Therefore, instead of the error in eq. 2 one should use the following error:

$$\epsilon_i = \tilde{q}_i - q_c({}^A T_c \ {}^c P_t \ {}^t T_e, \zeta_k) \tag{5}$$

In most cases there are not a linear relation between two frames, as we will prove in section III, the relation may be written as:

$$\epsilon_i = \tilde{q}_i - \mathcal{F}(q_c, \Psi, \zeta_k) \tag{6}$$

Where Ψ denotes the transformation indices. Calibration of a robot is an identification process, and hence, one should take a careful look at the identifiability of the model parameters; i.e. the regression must be linearly independent and the input signal must be persistently exciting. As the parameters in the function is not linear, linear methods like least-squares methods cannot be used. The nonlinear identifier must satisfies General Function Approximation (GFA) property which leads to orthogonality of sub-space kernels. Many Gradient based or free methods can be list here, but among them, Levenberg-Marquardt (LM algorithm) proved to be very successful in practice and is generally recommended to find the optimal solution [15]. Using this method, from Eq. 6, the iterative solution may be formulated as:

$$x_{j+1} = x_j - [J(x_j)^T \cdot J(x_j) + \mu_j . I]^{-1} \cdot J(x_j) \cdot b(x_j) \tag{7}$$

According to Marquardt suggestion, set $\mu_j = 0.001$ if x_j is the initial guess, set $\mu_j = \lambda(0.001)$ if $\|b(x_{j+1})\| \leq \|b(x_j)\|$, set $\mu_j = 0.001/\lambda$ if $\|b(x_{j+1})\| \geq \|b(x_j)\|$, and set λ to a constant parameter in the range of $2.5 < \lambda < 10$ [16].

III. Vision-Based Measurement

This section goes with proposing a method to obtain spatial coordinate of a point on a sphere. Since we have 3 degrees of freedom in a plane, in order to obtain the translation of the robot end-effector, one may consider a shape with corners to detect their intra-displacement. Here we just compute the translational motion of the rigid body with only a point as the marker on the robot end-effector. firstly, calibrate the camera to get the true position of environment, based on scene and lens parameters [8].

A. Camera Calibration

The most common model for photometric cameras is the pin-hole camera with perspective projection [8]. A range of information is lost in this projection, but the angle or orientation of the object point can be obtained if the focal length is known and the lens does not cause distortion.

The parameters which affect this mapping can be divided into three categories [17], [18]: (a) extrinsic (or external) parameters, which describe the relationship between the camera frame and the world frame, including position and orientation (six parameters); (b) intrinsic (or internal) parameters, which describe the characteristics of the camera, and include the lens focal length, pixel scale factors, and location of the image center; and (c) distortion parameters, which describe the geometric non-linearities of the camera. The six Extrinsic camera parameters are used to describe the orientation and position (three for each) of the camera coordinate system (X, Y, Z). They represent the relationship between the camera coordinates and the real world or object coordinates (X_W, Y_W, Z_W) [19]. The transformation from 3D coordinate (X, Y, Z) to the coordinates of the object point in the image plane follows the perspective equations below:

$$u = f\frac{x}{z} \ ; \ v = f\frac{y}{z} \tag{8}$$

Where f is the focal length. The image coordinates $(X; Y)$ are related to $(u; v)$ by the following equations [20]:

$$X = s_u v \ ; \ v = s_v v \tag{9}$$

Where s_u and s_v are scale factors accounting for TV scanning and timing effects and converting camera coordinates in millimeter or meters to image coordinates $(X; Y)$ in pixels.

B. Spherical Positioning

Here, we project a sphere in 3D space into a plane using a nonlinear transformation. As this transformation is a diffeomorphism, a nonlinear function exist to project these two surfaces. Since there is just two degree of freedom, this positioning requires only one camera, and therefore, it is grossly simpler and easy-to-apply rather than other methods. For the sake of simplicity, in the following equation the camera is assumed to be mounted on 45 degrees from base and in direction of the mechanism RCM (the optimal camera distance will be discussed later). After rejection of distortion and identification of intrinsic parameters according to previous section, we use equation 10 to 12 to obtain spherical coordinate of the system.

$$\begin{bmatrix} \phi \\ \gamma \end{bmatrix} = \begin{bmatrix} T_\phi(x) \\ T_\gamma(y) \end{bmatrix}, \tag{10}$$

$$\begin{aligned} T_\phi(x) &= \frac{\pi}{2} + \sin^{-1}(\frac{R+r}{R}\sin(\alpha) - \alpha), \\ T_\gamma(y) &= \frac{\pi}{4} + \sin^{-1}(\frac{R+r}{R}\sin(\delta) - \delta), \end{aligned} \tag{11}$$

where,

$$\begin{aligned} \alpha &= \tan^{-1}(\frac{\tan(\alpha_{max})}{n_x r^2}(x - n_x)), \\ \delta &= \tan^{-1}(\frac{\tan(\delta_{max})}{n_y r^2}(y - n_y)). \end{aligned} \tag{12}$$

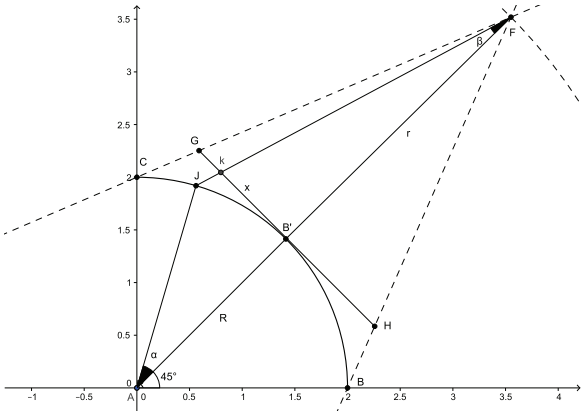

Fig. 1. Mapping an arch to a line in 45 deg

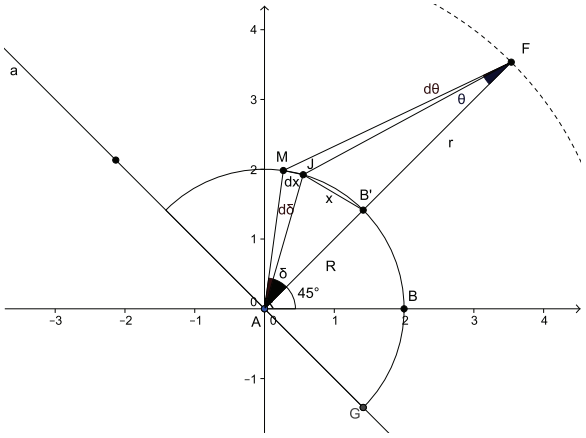

Fig. 2. Sensitivity of the measurements in π sector

In which, n_x, n_y are equal to number of pixel divided by 2, in each axis respectively, and $\alpha_{max}, \delta_{max}$ are the maximum available angle that camera can visit on the sphere surface.

C. Proof

In Fig. 1 Based on sine role in $\triangle AJF$ we have:

$$\frac{\sin(\beta)}{R} = \frac{\sin(\pi - \alpha - \beta)}{R + r} \tag{13}$$

For maximum detectable angle in γ axis we have:

$$\frac{\sin(\beta_{max})}{R} = \frac{\sin(\pi - \pi/4 - \beta_{max})}{R + r} \tag{14}$$

Then in $\triangle KB'F$ following equation coincide:

$$\begin{aligned} x &= kn_x \\ \tan(\beta_{max}) &= k\tfrac{n_x}{r} \end{aligned} \tag{15}$$

Where k is equal to the lens gain based on eq. 8, 9. Now we can find arbitrary point J in surface of sphere (regarding K):

$$\tan(\beta) = \frac{x}{r} = k(\frac{x - n_x}{r}) \tag{16}$$

To find β_{max} the equation 14 in $\triangle OJF$ we have:

$$\frac{\sin(\beta_{max})}{R} = \frac{1}{R + r} \tag{17}$$

Maximum detectable angle of the sphere is less than 180 degrees. This maximum range is preserved only if the camera is put into infinity that will deteriorate measuring precision. Furthermore, it can be shown that the nonlinearity increase if the angle increases from center (45 degree), In other word, in central area $\gamma \in [\pi/4 - \epsilon, \pi/4 + \epsilon], \phi \in [\pi/2 - \epsilon, \pi/2 + \epsilon]$ the transformation is almost linear. We will show the later one in the following sections.

IV. Calibration Attribute

In this section firstly, sensitivity of the measurement is described and then an optimization over location of the camera is performed to maximize prescribed benefit function.

A. Sensitivity Analysis

Consider a half of a circle in 1D that may easily generalized for the surface of a sphere. Equation 18 coincide based on sine role in $\triangle AB'J$, $\triangle FB'J$ in Fig. 2:

$$\begin{aligned} \frac{\sin(\delta)}{x} &= \frac{\sin(\frac{\pi-\delta}{2})}{R} \\ \frac{\sin(\theta)}{x} &= \frac{\sin(\frac{\pi-\delta}{2} - \theta)}{r} \end{aligned} \tag{18}$$

Joining these two equations will result:

$$\frac{\sin(\theta)}{\sin(\delta)} = \frac{R}{r}(\frac{\sin(\frac{\pi-\delta}{2} - \theta)}{\sin(\frac{\pi-\delta}{2})}) \tag{19}$$

Rewrite equation 19 in the following form:

$$\frac{\sin(\theta)}{sin(\delta)} = \frac{R}{r}\Big[cos(\theta) - tan(\frac{\delta}{2})\sin(\theta)\Big] \tag{20}$$

Now if we have a small increment $d\delta$, then we have similar discrepancies in $\triangle MAJ$, MJF, MAF as shown in Fig. 2:

$$\begin{aligned} \tfrac{\sin(d\delta)}{dx} &= \tfrac{\sin(\frac{\pi-d\delta}{2})}{R} \\ \tfrac{\sin(d\theta)}{dx} &= \tfrac{\sin(\gamma)}{r'} \\ \tfrac{\sin(\theta+d\theta)}{R} &= \tfrac{\sin(\delta+d\delta)}{r'} \end{aligned} \tag{21}$$

In which:

$$\begin{aligned} \gamma &= 2\pi - \frac{\pi - d\delta}{2} - \frac{\pi - \delta}{2} - (\frac{\pi - \delta}{2} - \theta) \\ &= \frac{\pi + d\delta}{2} + \delta + \theta \end{aligned} \tag{22}$$

By combining equation 22 and 21 with 20, we may have:

$$\sin(d\theta) = \Big(R\frac{\sin(d\delta)}{\sin(\frac{\pi-d\delta}{2})}\Big)\Big(\frac{\sin(\gamma)}{R}\frac{\sin(\theta + d\theta)}{\sin(\delta + d\delta)}\Big) \tag{23}$$

The later equation can be written in the form:

$$\frac{\sin(d\theta)}{\sin(d\delta)} = \frac{\cos(d\delta/2 + \delta + \theta)}{\cos(d\delta/2)}\frac{\sin(\theta + d\theta)}{\sin(\delta + d\delta)} \tag{24}$$

Finally,

$$\frac{s(d\theta)}{s(d\delta)} = \Big(c(\theta + \delta) - t(d\delta/2)s(\delta + \theta)\Big)\Big(\frac{s(\theta + d\theta)}{s(\delta + d\delta)}\Big). \tag{25}$$

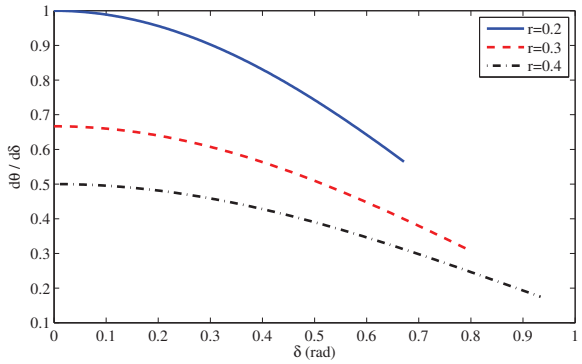

Fig. 3. Rate of changes in θ versus δ with constant R

Where s, c, t denote $\sin, \cos, \tan$, respectively. Now let's accept some approximation in equation 25 for the sake of simplification. The consideration are:

$$\begin{aligned} \frac{\sin(d\theta)}{\sin(d\delta)} &\approx \frac{d\theta}{d\delta} = \frac{\theta}{\delta} S_\delta^\theta \\ \frac{\sin(\theta + d\delta)}{\sin(\delta + d\delta)} &\approx \frac{\sin(\theta)}{\sin(\delta)} \end{aligned} \tag{26}$$

Where S_δ^θ denotes sensitivity of θ w.r.t δ. Finally:

$$S_\delta^\theta \approx \frac{R\delta}{r\theta}\Big[\Big(c(\theta+\delta) - t(d\delta/2)s(\delta+\theta)\Big)\Big(c\theta - t(\delta/2)s\theta\Big)\Big] \tag{27}$$

$$S_\delta^\theta \approx \frac{R\delta}{r\theta}\Big[\Big(c(\theta+\delta) - \epsilon\ s(\delta+\theta)\Big)\Big(c\theta - t(\delta/2)s\theta\Big)\Big] \tag{28}$$

In these equations we assume that the term $\tan(d\delta/2) = \epsilon$ is a small constant variable. According to equation 13, we can plot the sensitivity function w.r.t. δ and θ in Fig. 3, 4, with $R = 20\ cm$ and r is equal to $0.2, 0.3$ and $0.4\ (m)$.

According to Fig. 4, S_δ^θ for $r = 0.2\ (m)$ starts from 3, which means any change in the position of end-effector (around center) effects three time more on displacement of pixel in lens. It should be considered that if camera closed on the robot too much, less area will be visited due to the limitation of lens conical conerage . Therefore, a multi-objective optimization consist of sensitivity and coverage space based on user application can be defined to reach to a trade-off. In next section we will find a sub-optimal solution.

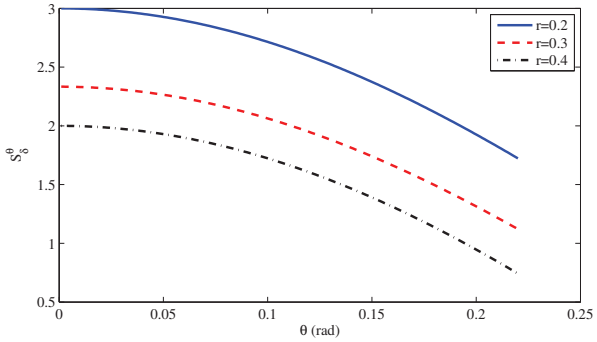

Fig. 4. Sensitivity with constant R

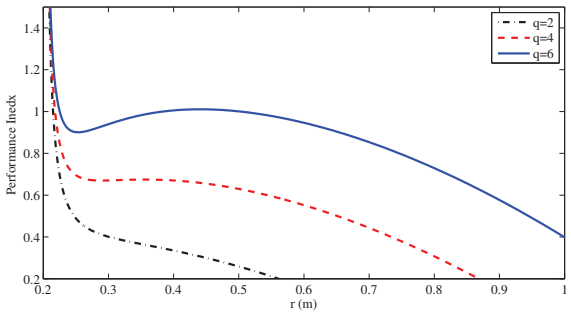

Fig. 5. Optimization for different weighting functional

B. Optimization

The optimization benefit function includes the region of interest and the loss area (background). As we have in follow:

$$J = q\ S_{ROI} - S_{waste} \tag{29}$$

In which, the coefficient q is a design parameter. Surface of interest can be calculated using spherical integration:

$$S_{ROI} = \int_0^{2\alpha}\int_0^{\beta} r^2 \sin(\theta) d\theta d\phi \tag{30}$$

Where r is the distance of camera from robot RCM which needs to be optimized and θ is the len's view angle. Without loss of generality, we assume that the region of interest is a half sphere. Hence, in equation 30 the term β is equal to π. Then the function can be simply modeled as:

$$J = 4q\alpha R^2 - \pi\left(r^2 \tan^2(\theta) - \frac{R^2}{\sin^2(\alpha)}\right) \tag{31}$$

It can be written as a function of R, r, θ by substitution $\cos(\alpha) = R/r$ the simple form can be derived as:

$$J = 4qR^2 \cos^{-1}(R/r) - \pi r^2\left(\tan^2(\theta) - \frac{R^2}{r^2 - R^2}\right) \tag{32}$$

Equation 32 depicts a multi-objective function for our problem. We can find the optimal solution analytically by mathematical programs such as MAPLE. The result can be simply given as:

$$\tan^2(\theta) R^{-4} = \frac{2q}{\pi A R r^2} - A^{-4} \tag{33}$$

Where $r^2 = A^2 + R^2$; the left hand sides denote the known terms that derives the problem to a nonlinear equation that can be solved using methods such as algebraic elimination, interval analysis, and continuation method [3], to find the roots of the polynomial. Benefit function is shown in Fig. 5 for 20 cm radius sphere with different weighings, in which the maximums may be solved analytically using eq. 33.

V. Experiments

A. Experimental Setup

In this section ARAS DIAMOND Eye surgery robot is calibrated as a case study for the proposed method. DIAMOND is a spherical mechanism in which all joint axes intersect at a point which represents the RCM of the mechanism. It has two pairs of identical spherical serial limbs that have common axes

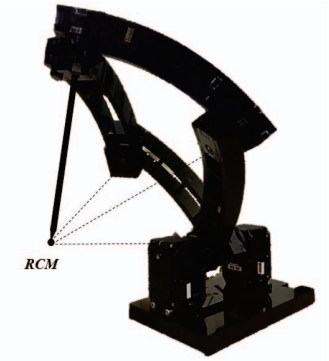

Fig. 6. DIAMOND ARAS Robot :a spherical parallelogram Eye surgery robot

at both ends (Fig. 6). The parallel structure of the mechanism provides inherent stiffness, which is appropriate for sensitive and precise applications such as eye surgery. Furthermore, dexterity and compact size of the robot is other benefits for such application. The workspace of the mechanism is a complete sphere that covers the region needed for vitroretinal surgeries [10]. The communication for the electronic hardware and the computer is through RS485 serial protocol using MATLAB RTW S-function in external mode. By this means an easy and reliable communication is generated with C-mex S-function as a medium for Simulink using kernel-based algorithms. Sampling rates restricted to 2.5 msec because of USB handshaking in full speed mode; rate transition (baud rate) is set to 3Mb/sec maximum available for motor ARMs. For the vision system a PS3 eye camera is used with 1280×640 resolution and 120 fps with a 6 mm lens. OpenCV library is used including Harris corner detection to find the corners. To have synchronized data between MATLAB and Qt, we use udp communication in local-host. The camera calibration is done based on hand-mounted camera robot calibration [21].

B. Identification

According to Fig. 7, the forward kinematic of DIAMOND in spherical coordinate are described as follows [10]:

$$\phi = \frac{\theta_1 + \theta_2}{2} \tag{34}$$

$$\gamma_{1,2} = 2\tan^{-1}\left(\frac{s\alpha\ cA \pm \sqrt{s^2\beta - (s\alpha\ sA)^2}}{c\alpha + c\beta}\right) \tag{35}$$

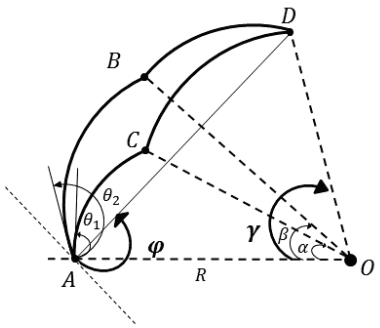

Fig. 7. Geometric representation of DIAMOND ARAS

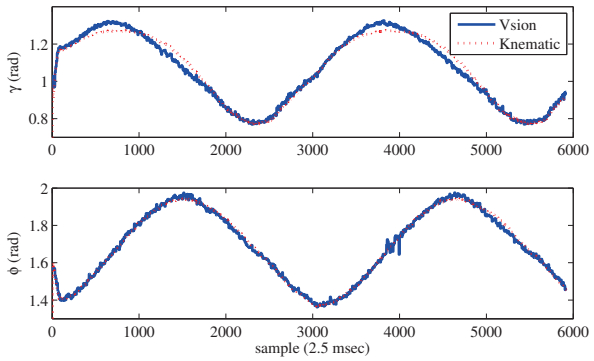

Fig. 8. Position from kinematics and vision

Where $A = (\theta_1 - \theta_2)/2$. By considering the collision between two limbs, only the positive sign solution of the equation in 35 may apply. According the the kinematic structure the following statements are coincide:

- Only γ axis includes kinematic parameters (α, β).
- We can use ϕ axis to find radius of the workspace.
- The variance of the error in the workspace can determine the RCM property of the manipulator.

The second statement states that by varying radius we can minimize the estimation error which is not directly appeared in kinematics as a parameter. The third statement is true since all the links are moved on the same surface of the sphere and consequently their pivots intersect at the sphere center. As the workspace of the robot is a quarter of a sphere, then term β in equation 30 must be equal to $\phi/2$. In the optimization problem, we choose the design coefficient equal to 5. The optimal distance is equal to 44.62 cm away from the RCM. The L.M. algorithm is used for nonlinear optimization, and columns of the identification Jacobian matrix are scaled with extremal scaling value to avoid biased estimation. The

TABLE I. A PRIORI AND IDENTIFIED KINEMATIC PARAMETERS

axis	$R\ (m)$	$\alpha\ (rad)$	$\beta\ (rad)$
a priori	0.2000	0.7854	0.7854
identified	0.2221	0.7634	0.8037

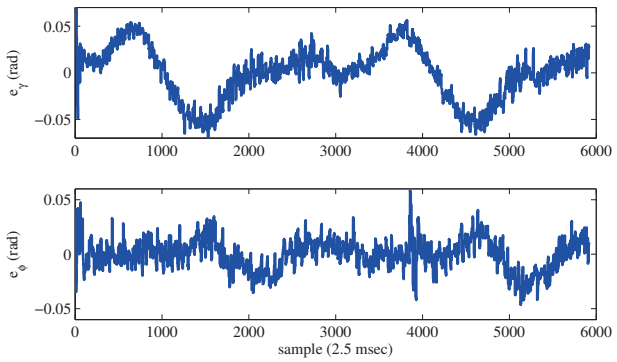

Fig. 9. Identification error

TABLE II. ERROR IN TASK SPACE (RAD)

parameters	ϕ	γ
mean error	-5.0400E-05	-3.8888E-05
RMS error	1.0882	1.9923
sup error	0.0591	0.0760

identified parameters are shown in table I; together with mean, root square mean (RMS) and maximum error in table II. Based on measurement setup and sensitivity, the calibration range is 0.050-to-2.100 rad = 0.021-to-1.047 rad or = 1-to-640 pxl.

C. Validation

Now we want to prove the enrichment of robot repeatability and accuracy using straightness evaluation. To confirm the previous results independently from the measuring device, an experiment is conducted, where by the same control structure, the projection of robot's moving-platform is lead to move along a line. Control Structure is a simple PD in Task-space with force distribution. The projection is the image of moving-platform from top view, where the camera's lens is parallel to the base. Since positioning of points in a line using vision is straightforward and does not need extrinsic and distortion parameter, this validation does not depend on measuring setup [19]. We conduct two scenarios for γ, ϕ axis as follows:

- case 1: (Vertical) $\phi = \pi/2$, $\gamma = \pi/6 \ : \ \pi/2$
- case 2: (Horizontal) $\gamma = \pi/4$, $\phi = \pi/3 \ : \ 2\pi/3$

The joint variables relationship in previous cases are $\theta_1 + \theta_2 = \pi$ and $\theta_1 - \theta_2 = \pi/2$ respectively. Straightness of the line is computed for the kinematic parameter sets (a priori and identified) as the root mean square of the distance between the different positions and the line estimated by a least squares criterion. The results are presented in Table III. Remaining error is because of control structure and measurement noise, that can be improved using model-based control schemes like inverse dynamic control.

VI. CONCLUSION

In this article, the kinematic calibration of the DIAMOND robot, a spherical parallel mechanism, using a vision-based measuring device were presented. Composed of a single camera, the vision system is low-cost, easy to use, and the pose measurement enables one to perform calibration using the standard calibration method based on the inverse kinematic model. Precision in the order of 0.01 rad for 2 translations in spherical coordinate have been obtained for a displacement of 1 rad. The accuracy improvement has been confirmed by Straightness validation experiments. These specifications may be improved by the use of available higher resolution CCD sensors, or by adding second camera to improve measurement performance.

TABLE III. VALIDATION

SSE	vertical (cm)	horizontal (cm)
uncalibrated	1.64	1.52
calibrated	0.62	0.59

ACKNOWLEDGMENT

The authors would like to thank the ARAS team particularly Arash Arjmandi and Amin Mahmodzadeh in the Department of Systems and Control for their helpful assistance along the way.

REFERENCES

[1] J. Swevers, C. Ganseman, D. Tukel, J. De Schutter, and H. Van Brussel, "Optimal robot excitation and identification," *Robotics and Automation, IEEE Transactions on*, vol. 13, pp. 730–740, Oct 1997.

[2] J. Wang and O. Masory, "On the accuracy of a stewart platform. i. the effect of manufacturing tolerances," in *Robotics and Automation, 1993. Proceedings., 1993 IEEE International Conference on*, pp. 114–120, IEEE, 1993.

[3] H. D. Taghirad, *Parallel robots: mechanics and control*. CRC press, 2013.

[4] H. Zhuang, J. Yan, and O. Masory, "Calibration of stewart platforms and other parallel manipulators by minimizing inverse kinematic residuals," *Journal of Robotic Systems*, vol. 15, no. 7, pp. 395–405, 1998.

[5] X. Li, J. Wang, N. Knight, and W. Ding, "Vision-based positioning with a single camera and 3d maps: accuracy and reliability analysis," *Journal of Global Positioning Systems*, vol. 10, no. 1, pp. 19–29, 2011.

[6] O. Henlich, "Vision-based positioning," May 1997.

[7] G. Van Albada, A. Visser, J. Lagerberg, and L. Hertzberger, "A portable measuring system for robot calibration," 1995.

[8] J. M. S. Motta, G. C. de Carvalho, and R. McMaster, "Robot calibration using a 3d vision-based measurement system with a single camera," *Robotics and Computer-Integrated Manufacturing*, vol. 17, no. 6, pp. 487–497, 2001.

[9] S. Charles, H. Das, T. Ohm, C. Boswell, G. Rodriguez, R. Steele, and D. Istrate, "Dexterity-enhanced telerobotic microsurgery," in *Advanced Robotics, 1997. ICAR'97. Proceedings., 8th International Conference on*, pp. 5–10, IEEE, 1997.

[10] A. Molaei, E. Abedloo, H. D. Taghirad, and Z. Marvi, "Kinematic and workspace analysis of diamond: An innovative eye surgery robot," in *Electrical Engineering (ICEE), 2015 23rd Iranian Conference on*, pp. 882–887, IEEE, 2015.

[11] H. Jean-Pierre, "Robotic eye surgery: Past, present, and future," *Journal of Computer Science & Systems Biology*, 2012.

[12] P. Renaud, N. Andreff, J.-M. Lavest, and M. Dhome, "Simplifying the kinematic calibration of parallel mechanisms using vision-based metrology," *Robotics, IEEE Transactions on*, vol. 22, no. 1, pp. 12–22, 2006.

[13] K. Schröer, S. L. Albright, and M. Grethlein, "Complete, minimal and model-continuous kinematic models for robot calibration," *Robotics and Computer-Integrated Manufacturing*, vol. 13, no. 1, pp. 73–85, 1997.

[14] P. Renaud, N. Andreff, F. Marquet, and P. Martinet, "Vision-based kinematic calibration of a h4 parallel mechanism," in *Robotics and Automation, 2003. Proceedings. ICRA'03. IEEE International Conference on*, vol. 1, pp. 1191–1196, IEEE, 2003.

[15] R. Bernhardt, R. Bernhardt, and S. Albright, *Robot calibration*. Springer Science & Business Media, 1993.

[16] J. E. Dennis Jr and R. B. Schnabel, *Numerical methods for unconstrained optimization and nonlinear equations*, vol. 16. Siam, 1996.

[17] B. Prescott and G. McLean, "Line-based correction of radial lens distortion," *Graphical Models and Image Processing*, vol. 59, no. 1, pp. 39–47, 1997.

[18] H. Zhuang and Z. S. Roth, *Camera-aided robot calibration*. CRC press, 1996.

[19] E. Church and A. O. Quinn, "Elements of photogrammetry," 1948.

[20] R. Y. Tsai, "A versatile camera calibration technique for high-accuracy 3d machine vision metrology using off-the-shelf tv cameras and lenses," *Robotics and Automation, IEEE Journal of*, vol. 3, no. 4, pp. 323–344, 1987.

[21] J. Weng, P. Cohen, and M. Herniou, "Camera calibration with distortion models and accuracy evaluation," *IEEE Transactions on pattern analysis and machine intelligence*, vol. 14, no. 10, pp. 965–980, 1992.